Journal of Alloys and Compounds 847 (2020) 156541

Contents lists available at ScienceDirect

Journal of Alloys and Compounds

journal homepage: http://www.elsevier.com/locate/jalcom

Er^{3+}/Ho^{3+} codoped nanogarnet as an optical FIR based thermometer for a wide range of high and low temperatures

K. Soler-Carracedo [a, *], I.R. Martín [a, b], F. Lahoz [a, c], H.C. Vasconcelos [d, e], A.D. Lozano-Gorrín [b, f], L.L. Martín [a], F. Paz-Buclatin [a]

[a] Departamento de Física, Universidad de La Laguna, Av. Astrofísico Francisco Sánchez, s/n, 38200 La Laguna, Tenerife, Spain
[b] Instituto Universitario de Materiales y Nanotecnología (IMN), Universidad de La Laguna. Santa Cruz de Tenerife, Tenerife, Spain
[c] Instituto Universitario de Estudios Avanzados en Atómica, Molecular y Fotónica (IUdEA), Universidad de La Laguna. Santa Cruz de Tenerife, Tenerife, Spain
[d] Faculty of Sciences and Technology, Azores University, Ladeira da Mãe de Deus, Ponta Delgada, Portugal
[e] Centre of Physics and Technological Research (CEFITEC), FCT/UNL Faculdade de Ciências e Tecnologia, Caparica, Portugal
[f] Departamento de Química, Universidad de La Laguna. Av. Astrofísico Francisco Sánchez, s/n, 38200 La Laguna, Tenerife, Spain

ARTICLE INFO

Article history:
Received 22 June 2020
Received in revised form
23 July 2020
Accepted 24 July 2020
Available online 30 July 2020

Keywords:
Optical sensing
High and low temperatures
Nanogarnet

ABSTRACT

In this work, a new strategy to increase the temperature working range of rare-earth based optical thermometers is demonstrated. Nanocrystalline yttrium gallium nanogarnets codoped with 0.1% Er^{3+} and 0.1% Ho^{3+} were synthesized. The codoped samples combine the high performance of erbium ions at high temperatures and that of holmium ions at low temperature, providing an overall relatively high sensor performance in a temperature range from 30 to 540 K, broader than that achievable by single Er^{3+} or Ho^{3+} doped nanogarnets. Measurements were carried out using 406 and 473 nm commercial diode lasers to excite the erbium and holmium ions, respectively. The emission spectra were analyzed as a function of temperature, using the fluorescence intensity ratio technique for each ion. Relative sensitivity and limit of detection were obtained in order to compare the efficiency of the sensor with optical thermometers reported up to date, capable of working in a similar range from cryogenic to high temperatures. The sensor presents a maximum relative sensitivity of about 1.3% K^{-1} at 200 K when exciting the erbium ions and around 0.4% K^{-1} at 200 K for the holmium ions. The limit of detection is under 0.5 K for most of the range from 30 K to 540 K using this combination of ions.

1. Introduction

The field of optical temperature sensors has gained increasing attention over the last decade as new technologies require more and more accurate and free-contact temperature sensing mechanisms [1–4]. In the family of phosphors used for these sensors, rare earths (RE) have become a fundamental element due to their photostability, among other important spectroscopic advantages. This type of sensors can be calibrated following a series of parameters such as variations of the decay time, the bandwidth, the positions of an emission band, or by using the fluorescence intensity ratio (FIR) technique [4]. These techniques present a series of advantages and drawbacks. This work will be focused on the use of the FIR technique which presents the advantages of reducing the influence of the measurement conditions as well as improving the sensitivity of the measurements. Compared to decay time based sensor, the FIR setup requirements are less demanding and do not require great resolution [5], as it only needs to compare the intensity of two emission bands. Moreover, higher thermal resolution is reported using FIR rather than changes in the emission bandwidth or spectral position [4–6].

Many research groups have been studying the RE fluorescence intensity response as a function of temperature, focusing in the development of different host matrices and the analysis of more efficient and reliable RE dopant candidates [4,7–10]. Garnet crystal is a common gain media in laser applications due to their good thermal and optical properties as well as high mechanical strength [11]. In particular, they are popular due to their high thermal conductivity and density, good chemical stability, high isotropy, relative low-energy phonons, and great transparency from the ultraviolet (UV) to the mid infra-red (IR) region [11]. All of these

* Corresponding author. Departamento de Física, Universidad de La Laguna, Av. Astrofísico Francisco Sánchez, s/n, 38200 La Laguna, Tenerife, Spain.
E-mail address: ksolerca@ull.edu.es (K. Soler-Carracedo).

https://doi.org/10.1016/j.jallcom.2020.156541
0925-8388/

properties make this family of materials one of the most important host matrices for trivalent RE ions, with the Nd^{3+} doped $Y_3Al_5O_{12}$ (YAG) garnet considered as a standard for laser material.

Regarding the election of RE candidates, erbium is the most common, due to the presence of the thermally coupled levels $^2H_{11/2}$ and $^4S_{3/2}$, whose energy gap is relatively close to the thermal energy at RT. Moreover, it also presents relatively high radiative emitting efficiencies to ground or first excited states [12]. Due to these advantages, Er^{3+} doped materials have been extensively studied [5,13–19] since its first report as a temperature sensor based on the FIR technique in 1990 [20]. However, the main disadvantage is that the $^2H_{11/2}$ thermal population decreases at low temperatures, making the use of FIR technique for Er^{3+} ions inaccurate. On the other hand, $^5F_4$ and $^5S_2$ excited energy levels of Ho^{3+} ions are so close that they are thermally coupled even at cryogenic temperatures. Compared to erbium, holmium ions have generally not been considered for temperature sensors until recent years, used mainly as a codopant for temperature sensors based on up-conversion processes [17,21–25].

The vast majority of optical temperature sensors only cover ranges of high temperatures (from RT to approximately 500 K) or low temperatures (from cryogenic to RT). There are only few reports on optical materials capable of measuring in both ranges, from cryogenic to over 500 K [4,26]. In this work, a temperature sensor is developed based on the work of P. Haro-Gonzalez et al. in 2011 [27], where they measured in the aforementioned range two different fluoroindate glass samples, one doped with Er^{3+} and the other with Ho^{3+}. Following this idea, a yttrium-gallium nanogarnet codoped with erbium and holmium has been synthesized, with low dopant concentration (only 0.1 mol%) to minimize the energy transfer between the two ions [28]. Indeed, energy transfer processes strongly depend on the ion-to-ion distance. Therefore, a low dopant concentration increases the average interionic distance and, consequently, severely decreases the energy transfer probability. In this way, Er^{3+} and Ho^{3+} dopants can be independently excited. Therefore, this novel material is able to work as a FIR based temperature nanosensor in a wide range of temperatures from 30 K to 540 K. The strategy of the independent ion excitation provides the advantage of the high performance of Er^{3+} and Ho^{3+} ions in the high and low temperature ranges, respectively.

2. Theoretical background

2.1. Technique

The FIR technique is based on temperature-related changes in the fluorescence intensity ratio of transitions from two thermally coupled excited states of RE ions. This allows a calibration to be done to estimate the temperature of the sample from the intensity ratio of the mentioned emissions. The population of both levels involved in the process is proportional to the pump power of the incident source. As a consequence, the ratio of the intensities is independent of the source power intensity and only depends on temperature changes.

In the case of Er^{3+} ions, the optical temperature sensor can be analyzed as a three-level system, in which $^2H_{11/2}$ and $^4S_{3/2}$ levels are thermally coupled.

For low pump power excitation, avoiding sample heating, the emission intensity ratio (Δ) between the two emitting levels (E_2, E_3) can be described as a Boltzmann type distribution [29]:

$$\Delta(T) = \frac{I_{3-1}}{I_{2-1}} = \frac{\omega_{31}^R g_3 h\nu_3}{\omega_{21}^R g_2 h\nu_2} \exp\left(\frac{-E_{32}}{K_B T}\right) = Cexp\left(\frac{-E_{32}}{K_B T}\right) \quad (1)$$

where I_{3-1} is the emission intensity of the transition from level 3 to level 1, I_{2-1} is the emission intensity of the transition from level 3 to level 2, K_B is the Boltzmann constant, E_{32} is the energy gap between the two thermalized excited levels 2 and 3, g_3 and g_2 are the degeneracies $(2J+1)$ of these levels, ν_3 and ν_2 are the frequencies of the transitions from level 3 and 2 to ground state respectively and ω_{31}^R and ω_{21}^R are the spontaneous emission rates from the respective levels to the ground state (E_1) and C is the pre-exponential factor. Recording the ratio of emission intensity of the nearby levels as a function of temperature, the data can be fitted to Eq. (1).

Whereas for the Ho^{3+}, the coupled levels $^5S_2$ and $^5F_4$ are also thermalized with a very small gap. Therefore, it is not possible to separate the contribution of the emission coming from each level. But, the ratio corresponding to the $^5S_2(^5F_4) \rightarrow {}^5I_8$ and $^5S_2(^5F_4) \rightarrow {}^5I_7$ transitions has an important temperature dependence [30].

2.2. Sensitivity

The absolute thermal sensitivity (S) of the optical temperature sensor describes the rate of change of the thermometric parameter; which, in this case, corresponds to the emission intensity ratio in response to temperature variations and it is given by:

$$S = \left|\frac{d\Delta}{dT}\right| \quad (2)$$

However, this feature depends on the nature of the thermometric parameter, the experimental setup as well as the dopant and active matrix of the thermometric material. Thus, in order to compare different thermometers, Collins et al. [8] in 1998 define another figure of merit called the relative sensitivity (S_r) given as:

$$S_r = \frac{1}{\Delta}\left|\frac{d\Delta}{dT}\right| \quad (3)$$

which allows comparison of optical sensors performances, even if they use different physical parameters to detect a temperature change.

Another important parameter used to characterize the sensor is the limit of detection (δT_{min}), also known as temperature uncertainty. This parameter is related to the minimum temperature change that the sensor is capable to register and it is given as:

$$\delta T_{min} = \frac{1}{S_r}\frac{\delta\Delta}{\Delta} \quad (4)$$

where $\delta\Delta/\Delta$ is the resolution limit or relative uncertainty of the thermometric parameter, that is, the smallest change in ratio that can be experimentally detected. The resolution limit is related to the thermometer performance but is also dependent on the experimental setup [31]. Therefore, one way to improve the resolution limit could be the use of better acquisition systems as well as to improve measurement performance, for example, by increasing integration time and using the average of consecutive measurements to decrease experimental noise.

3. Experimental

3.1. Sample preparation

Er3+/Ho3+-codoped nanocrystalline yttrium gallium nanogarnets (YGG), with the formula $Y_{2.8}Er_{0.1}Ho_{0.1}Ga_5O_{12}$, were successfully synthesized by the citrate sol-gel method in air atmosphere. Stoichiometric molar ratios of high-purity $Ga(NO3)_3{\cdot}9H2O$ (Sigma-Aldrich, 99.99%), $Y(NO3)_3{\cdot}4H2O$ (Sigma-Aldrich, 99.99%),

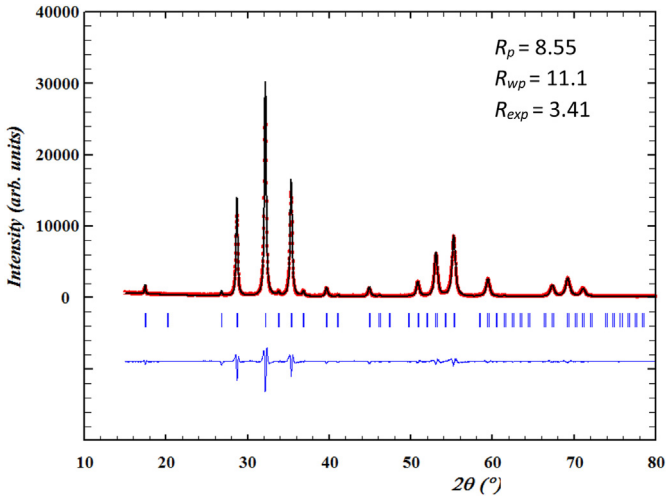

Fig. 1. Rietveld fitting of the XRD pattern for $Y_{2.8}Er_{0.1}Ho_{0.1}Ga_5O_{12}$ nanogarnet. The difference pattern (blue) between calculated (black line) and observed (red dots) has been included. The vertical lines correspond to the Bragg positions allowed for the *Ia-3d* space group. (For interpretation of the references to colour in this figure legend, the reader is referred to the Web version of this article.)

$Er(NO3)_3 \cdot 5H2O$ (Sigma-Aldrich, 99.99%) and $Ho(NO3)_3 \cdot 5H2O$ (Sigma-Aldrich, 99.99%) reagents were dissolved in 50 ml of HNO_3 1:1 under stirring at 363 K for 3 h. Citric acid, with a molar ratio of metal ions to citric acid of 1:2, was then added to the solution and heated at the same temperature till gel formation. The resulting gel was heated at 673 K for 6 h to remove the residual nitrates and the organic compounds. The obtained precursor was then heated at 1123 K for 14 h to finally obtain the wanted material. Powder X-ray diffraction data was collected to ensure that the synthesis was successful on a PANalytical X'Pert PRO diffractometer (Bragg-Brentano geometry) with an X'Celerator detector employing the Cu Kα1 radiation (λ = 1.5405 Å) in the angular range $5° < 2\theta < 80°$, by continuous scanning with a step size of 0.002°.

3.2. Optical characterization

The absorption spectrum of the sample was measured with a double beam spectrophotometer (Cary Series UV–vis–NIR Spectrophotometer from Agilent Technologies). The emission spectra were obtained by exciting with commercial diode lasers at 406 nm to excite erbium ions or at 473 nm to excite holmium ions. To excite both ions simultaneously, an Oriel Xenon 400 W lamp with a monochromator was used. The emissions were focused onto an optical fiber, coupled to a 0.303 m grating single spectrometer (Andor Shamrock SR-303i-A) and detected with a cooled Newton CCD camera. All spectra were corrected from the spectral response of the equipment.

Measurements from RT to 540 K were carried out in a tubular electric furnace (Gero RES-E 230/3), where the temperature of the sample was controlled via a type K thermocouple in contact with it. For temperatures in the range of 30 K to RT, the samples were cooled in a continuous flow helium closed-cycle APD cryostat.

4. Results and discussion

Rietveld refinement of the X-ray diffraction (XRD) pattern is shown in Fig. 1. The obtained agreement factors (*R* factors) inset into it confirm the goodness of the fitting. The fitting has been carried out by considering the cubic symmetry with the space group *Ia-3d* (#230), obtaining a value of the cell parameter $a = 12.4365\ (3)$ Å. Besides, an accurate matching of the obtained XRD pattern and that for the corresponding garnet from the ICDD database [file number 04-009-8400] confirms once again the cubic symmetry with the space group *Ia-3d* (#230).

The average crystallite size has been estimated to be around 29.4 nm from the full width at half maximum (FWHM) of the diffraction peak at 32.22 °2θ (FWHM = 0.2814 °2θ) using the Scherrer equation along with the structure of the garnet unit cell. The Scherrer equation can be written as $\tau = \frac{K\lambda}{\beta cos\theta}$, where τ is the average crystallite size, K is the so-called shape factor and is generally taken as being about 1 for spherical particles, β is the FWHM in radians and θ is the Bragg angle.

Fig. 2 shows the absorption spectrum of the sample. Narrow absorption bands of both erbium and holmium ions are observed and assigned to their respective transitions [32]. The sharp peak profiles found in all electronic transitions confirm that both ions have been incorporated successfully in the crystalline garnet structure of the nanoparticles.

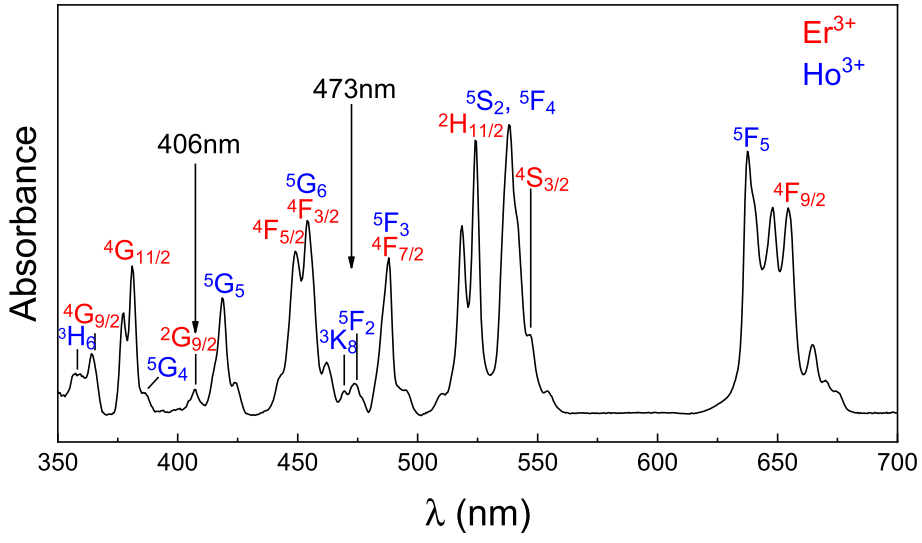

Fig. 2. Absorption spectrum of the YGG nanogarnet codoped with 0.1% Er^{3+} and 0.1% Ho^{3+}. The peaks correspond to transitions from the $^4I_{15/2}$ and $^5I_8$ to the indicated level of the Er^{3+} and Ho^{3+} ions, respectively. The arrows indicate the wavelengths selected to independently excite the Er^{3+} or Ho^{3+} ions.

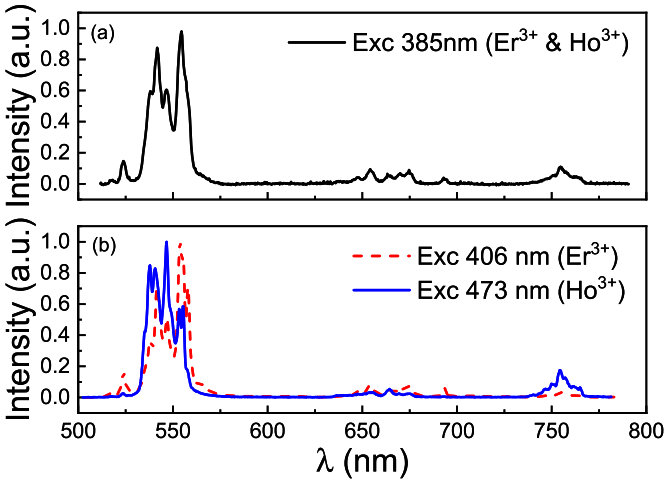

Fig. 3. Emission spectrum of the sample exciting the codoped ions simultaneously at 385 nm (a) and independently at 406 nm for Er^{3+} and at 473 nm for Ho^{3+} (b).

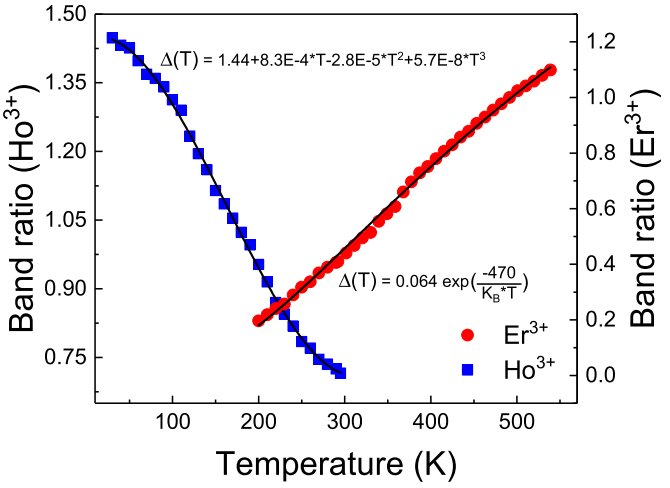

Fig. 4. FIR as a function of temperature of the $^2H_{11/2} \rightarrow {}^4I_{15/2}/{}^4S_{3/2} \rightarrow {}^4I_{15/2}$ erbium (red circles) transitions and the $^5S_2(^5F_4) \rightarrow {}^5I_8/{}^5S_2(^5F_4) \rightarrow {}^5I_7$ holmium (blue squares) transitions. (For interpretation of the references to colour in this figure legend, the reader is referred to the Web version of this article.)

When the sample is irradiated at 406 nm, the $^4I_{15/2} \rightarrow {}^2G_{9/2}$ erbium transition is excited. The emission spectrum under 406 nm excitation shows the typical erbium bands centered at 523 nm, 550 nm and a small band at 660 nm that correspond to the $^2H_{11/2} \rightarrow {}^4I_{15/2}$, $^4S_{3/2} \rightarrow {}^4I_{15/2}$ and $^4F_{9/2} \rightarrow {}^4I_{15/2}$ transitions, respectively (Fig. 3a). No significant holmium emission is detected.

On the other hand, when the $^5I_8 \rightarrow {}^5F_2$ holmium transition is excited at 473 nm, the emission spectrum changes, showing holmium bands centered at 540 nm and 750 nm (Fig. 3a), corresponding to the $^5S_2(^5F_4) \rightarrow {}^5I_8$ and $^5S_2(^5F_4) \rightarrow {}^5I_7$ transitions, respectively, due to the two thermally coupled levels $^5S_2$ and $^5F_4$. In addition to these, there is a small emission band centered at about 655 nm due to the $^5F_5 \rightarrow {}^5I_8$ transition.

Due to the large amount of Er:Ho:YGG absorption bands, when the sample is irradiated using broad-band excitation provided by a lamp, instead of a laser, it is possible to simultaneously excite both Er^{3+} and Ho^{3+} ions. As an example, a Xenon lamp was used for broad-band excitation around 385 nm. Under those conditions, both ions were simultaneously excited and the emission spectrum at RT is shown in Fig. 3b.

These results confirm that under 406 or 473 nm laser excitation, Er^{3+} and Ho^{3+} ions are independently excited, respectively. We believe that the low dopant concentration used in the YGG nanogarnets is essential to avoid significant energy transfer processes between both ions.

Upon Er^{3+} ions excitation at 406 nm, the positions of the Er^{3+} emission bands do not change with the temperature. However, the ratio of their emission intensities does, particularly for the 523 nm and 550 nm emission bands, corresponding to emissions from the $^2H_{11/2}$ and $^4S_{3/2}$ excited states, respectively, since the small gap between these two levels allows thermalization processes to occur. However, below 90 K the 523 nm emission band is hardly detectable because the population of the $^2H_{11/2}$ state is negligible as compared to that of the $^4S_{3/2}$ level. Consequently, the dependence of FIR with temperature has been measured from 100 to 540 K. The results are given in Fig. 4. FIR of the Er^{3+} emission bands increases as T is augmented. The dependence of FIR on temperature can be described by Eq. (1). Considering $^4I_{15/2}$, $^4S_{3/2}$ and $^2H_{11/2}$ as level 1, 2 and 3, respectively. A parameter of $E_{32} = 470\ cm^{-1}$ was obtained from the fitting.

Regarding the Ho^{3+} ions, the intensity ratio as a function of the temperature was obtained using the emissions at 550 and 750 nm. They correspond to the transition from the $^5S_2(^5F_4)$ thermalized excited states to the $^5I_8$ and $^5I_7$ levels, respectively. In this case, the energy gap between $^5S_2$ and $^5F_4$ states is smaller than the gap described for the excited levels of the Er^{3+} ions. Indeed, $^5S_2$ and $^5F_4$ energy levels are thermalized even at the lowest temperature of 30 K used in our experiments. Unlike the FIR behaviour of the Er^{3+} ions, the Ho^{3+} FIR emission bands decreases as temperature increases. Moreover, the highest temperature dependence occurs from 30 K to room temperature (RT). At temperatures higher than RT the change of FIR with temperature considerably diminishes. Therefore, we focused on the 30–300 K temperature range. See Fig. 4. The FIR results has been fitted to a cubic polynomial, and its coefficients are given in Fig. 4.

The relative sensitivity of the sensor has been evaluated using Eq. (3) and the FIR provided in Fig. 4 as a function of temperature. Taking advantage of the capability of the sample to independently

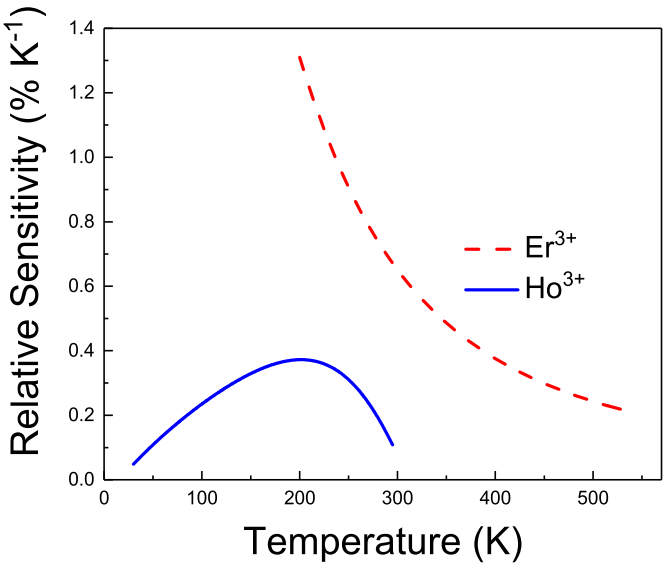

Fig. 5. Sensor relative sensitivity for the YGG nanogarnet exciting the erbium (red, dashed) and holmium (blue, continuous) transitions, independently. (For interpretation of the references to colour in this figure legend, the reader is referred to the Web version of this article.)

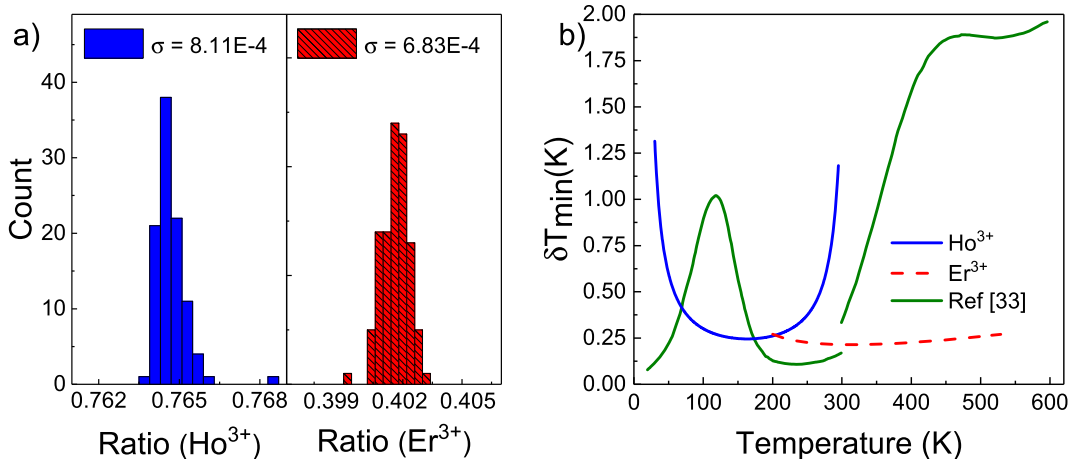

Fig. 6. a) Standard deviations obtained from the ratio of 100 measurements at RT for Er^{3+} ions and 250 K for Ho^{3+} ions. b) Respective limits of detection obtained using Eq. (4) and limit of detection obtained by Brites et al. [33].

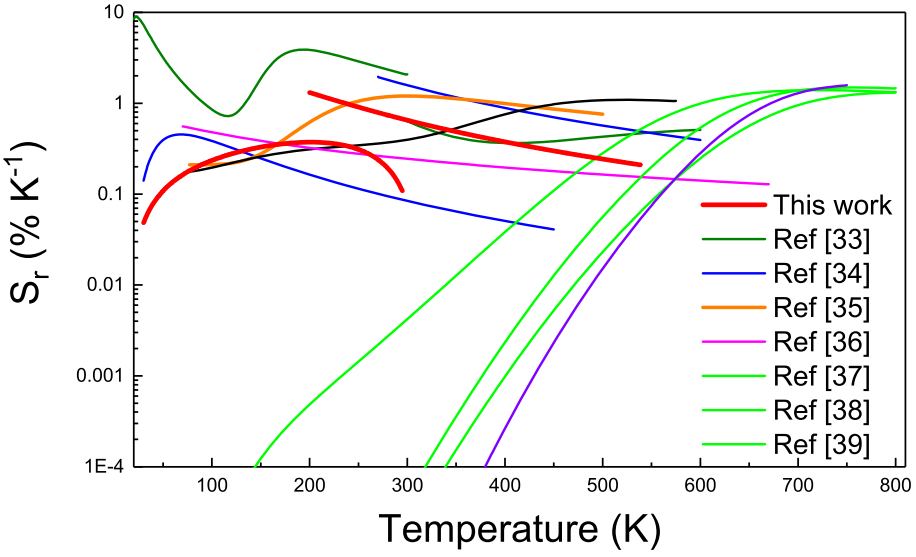

Fig. 7. Relative sensitivities of all RE based optical temperature sensors capable of covering a range from cryogenic to high temperatures.

excite Er^{3+} or Ho^{3+} ions, S_r has been calculated for both ion emissions. In the case of the Er^{3+} ions, S_r increases from about 0.2% K^{-1} at 540 K up to 1.3% K^{-1} at 200 K, which is the lowest temperature detected with the FIR technique. However, this technique can be applied to the Ho^{3+} ions emissions at lower temperature. Indeed, S_r has been calculated from 30 to 300 K for the Ho^{3+} ions, showing a maximum around 0.4% K^{-1} at 200 K (see Fig. 5).

In order to determine the limit of detection, 100 measurements were carried out in the same conditions at RT [31] for erbium and holmium ions. FIR was calculated for the 100 measurements and the FIR uncertainty ($\delta\Delta$) was taken as the standard deviation of the statistical distribution (Fig. 6a). For the excitation of erbium ions the standard deviation showed a value of $6.83 \cdot 10^{-4}$ and for the excitation of holmium ions the value was of $8.11 \cdot 10^{-4}$. The resulting limit of detection using Eq. (4) is presented in Fig. 7 b. Consequently, the temperature resolution of the sensor is below 0.5 K in almost all the range from 30 to 540 K temperature range using both Er^{3+} or Ho^{3+} FIR procedure.

In order to compare with other optical sensors, all RE based optical temperature sensors capable of covering a similar temperature range, from cryogenic to over 500 K, were summarized in Table 1, and their respective relative sensitivities were represented in Fig. 7. In comparison to other optical temperature sensors, YGG nanogarnets codoped with Er^{3+} and Ho^{3+} ions show high relative sensitivity values at low temperatures whereas, for high temperatures, the values are similar to those found in the literature, excluding decay time based sensors. In general, decay time based sensors show better relative sensitivities over 500 K than FIR or bandwith based sensors. However, below 300 K, their sensitivity quickly decay to near zero values. The highest relative sensitivity value recorded to date is $Sr_2GeO_4:Pr^{3+}$ crystalline powders by C. D. Brites et al. [33]. This material based in praseodymium used the intra and interconfigurational transitions to measure below and above 300 K, respectively. YGG:Er, Ho nanogarnets on the other hand, present much better limit of detection values, with values below 0.5 K from 60 K to 540 K, whereas for $Sr_2GeO_4:Pr^{3+}$ the values go up to around 1 K at 150 K and 2 K at 600 K (Fig. 6b). Furthermore, $Sr_2GeO_4:Pr^{3+}$ must be excited in the UV, whereas YGG nanogarnets on the other hand can be excited with low-cost commercial diode laser in the Vis range.

Table 1
List of lanthanide based thermometers capable of covering a wide range of high and low temperatures.

Material	T Range (K)	S_R (% K^{-1})	Optical parameter	Ref.
Sr_2GeO_4:Pr^{3+} crystalline powders	17–600	9 (31 K)	FIR	[33]
La2O2S:Nd3+ phosphors powder	30–600	1.95 (270 K)	FIR	[34]
Gd_2O_3:Eu^{3+} nanopowder	10–800	1.58 (750 K)	Decay time	[35]
$GdVO_4$:Eu^{3+}	10–750	1.48 (765 K)	Decay time	[36]
YGG:Er^{3+}/Ho^{3+} nanocrystalline garnets	10–540	1.3 (200 K)	FIR	This Work
La_2MgTiO_6:Pr^{3+} crystalline powders	77–500	1.28 (350 K)	FIR	[37]
AlO_3:Cr Ruby fiber	77–800	1.2 (675 K)	Decay time	[38]
$Ca_2YZr_2Al_3O_{12}$:Bi^{3+},Eu^{3+} phosphors	297–573	0.66 (548 K)	FIR	[39]
Y_2O_3:Eu^{3+} polycrystalline powders	10–670	0.56 (70 K)	Bandwith	[40]
YP_5O_{14}:Nd^{3+}	77–700	X	Decay time	[41]
$Eu(PO_3)_3$ glass	80–690	X	Decay time	[42]
AlN:Eu^{3+} implanted thin films	12–830	X	FIR	[43]
AlN:Tb^{3+} implanted thin films	12–830	X	FIR	[43]
AlN:Tm^{3+} implanted thin films	12–830	X	FIR	[43]
AlN:Pr^{3+} implanted thin films	12–830	X	FIR	[43]

5. Conclusions

In summary, YGG nanogarnets codoped with 0.1% Er^{3+} and Ho^{3+} were successfully synthesized by citrate sol-gel and characterized as temperature sensors. Due to the low concentration of both dopant ions, it is possible to excite each ion independently using two low-cost diode lasers without significant energy transfer processes between the ions. The FIR technique has been used to detect changes in temperature. In the case of Er^{3+} ions, FIR was applied to the $^2H_{11/2} \rightarrow {}^4I_{15/2}$ and $^4S_{3/2} \rightarrow {}^4I_{15/2}$ transitions from 100 up to 540 K. At temperatures below 100 K the thermal population of the $^2H_{11/2}$ excited state is negligible and FIR cannot be accurately determined. However, for the Ho^{3+} ions FIR was calculated from the emissions associated to the $^5S_2(^5F_4) \rightarrow {}^5I_8$ and $^5S_2(^5F_4) \rightarrow {}^5I_7$ electronic transitions. As the energy gap between $^5S_2$ and $^5F_4$ excited states is lower than of the used Er^{3+} excited levels, they are thermally coupled even at the lowest cryogenic temperature used in this study. Therefore, FIR could be obtained from 30 to 300 K. Consequently, the use of Er^{3+} and Ho^{3+} doped YGG nanogarnets enlarges the sensor temperature range that could be available using single doping. The relative sensitivity of the temperature sensor was determined both for the Er^{3+} and Ho^{3+} ions, showing a maximum of 1.3 and 0.4% K^{-1} at 200 K, respectively. The limit of detection in the temperature range from 30 to 540 K is below 0.5 K for most of the range. In order to compare the efficiency of our material, a comparative research was made to review all other RE optical temperature sensors that have been tested for a similar range of temperatures (from cryogenic to over 500 K). Our sample proved to have relatively high relative sensitivity values for low temperature and similar values for higher temperatures compared to the other sensors, as well as the best precision to date in a wider range than any of them, making erbium-holmium codoped nanogarnets a promising candidate as an optical temperature sensor.

CRediT authorship contribution statement

K. Soler-Carracedo: Writing - original draft, Data curation, Investigation. **I.R. Martín:** Conceptualization, Project administration. **F. Lahoz:** Formal analysis, Writing - review & editing. **H.C. Vasconcelos:** Data curation, Supervision. **A.D. Lozano-Gorrín:** Synthesis. **L.L. Martín:** Methodology. **F. Paz-Buclatin:** Investigation.

Declaration of competing interest

The authors declare that they have no known competing financial interests or personal relationships that could have appeared to influence the work reported in this paper.

Acknowledgements

The authors wish to thank financial support from MINECO (MAT2016-79866-R, MAT2016-75586-C4-4-P, FIS2017-82855-P, PID2019-107335RA-I00, PID2019-110430GB-C21, PID2019-106383 GB-C44), AEI (IJCI-2016-30498) and EU-FEDER.

References

[1] N. Nazarova, Y. Avlasevich, K. Landfester, S. Baluschev, All-optical temperature sensing in organogel matrices via annihilation upconversion, ChemPhotoChem 3 (2019) 1020–1026, https://doi.org/10.1002/cptc.201900093.
[2] J. Zhang, B. Ji, G. Chen, Z. Hua, Upconversion luminescence and discussion of sensitivity improvement for optical temperature sensing application, Inorg. Chem. 57 (2018) 5038–5047, https://doi.org/10.1021/acs.inorgchem.8b00102.
[3] A. Siaï, P. Haro-González, K. Horchani Naifer, M. Férid, Optical temperature sensing of Er^{3+}/Yb^{3}+ doped $LaGdO_3$ based on fluorescence intensity ratio and lifetime thermometry, Opt. Mater. 76 (2018) 34–41, https://doi.org/10.1016/j.optmat.2017.12.018.
[4] C.D.S. Brites, S. Balabhadra, L.D. Carlos, Lanthanide-based thermometers: at the cutting-edge of luminescence thermometry, Adv. Opt. Mater. 7 (2019) 1–30, https://doi.org/10.1002/adom.201801239.
[5] B. Dong, T. Yang, M.K. Lei, Optical high temperature sensor based on green upconversion emissions in Er^{3+} doped Al_2O_3, Sensor. Actuator. B Chem. 123 (2007) 667–670, https://doi.org/10.1016/j.snb.2006.10.002.
[6] M. Runowski, Pressure and temperature optical sensors: luminescence of lanthanide-doped nanomaterials for contactless nanomanometry and nanothermometry, in: Handb. Nanomater. Anal. Chem., Elsevier, 2020, pp. 227–273, https://doi.org/10.1016/B978-0-12-816699-4.00010-4.
[7] S. Uchiyama, A. Prasanna de Silva, K. Iwai, Luminescent molecular thermometers, J. Chem. Educ. 83 (2006) 720–727, https://doi.org/10.1021/ed083p720.
[8] S.F. Collins, G.W. Baxter, S.A. Wade, T. Sun, K.T.V. Grattan, Z.Y. Zhang, A.W. Palmer, Comparison of fluorescence-based temperature sensor schemes: theoretical analysis and experimental validation, J. Appl. Phys. 84 (1998) 4649–4654, https://doi.org/10.1063/1.368705.
[9] J. Zhou, S. Wen, J. Liao, C. Clarke, S.A. Tawfik, W. Ren, C. Mi, F. Wang, D. Jin, Activation of the surface dark-layer to enhance upconversion in a thermal field, Nat. Photon. 12 (2018) 154–158, https://doi.org/10.1038/s41566-018-0108-5.
[10] T. Katsumata, N. Kawaguchi, Y. Fujimaki, Y. Kiyokawa, H. Aizawa, S. Komuro, T. Morikawa, E. Toba, Rare-earth aluminate crystals for fluorescence thermometer application, in: SICE 2004 Annu. Conf., IEEE, 2004, pp. 2512–2515.
[11] V. Monteseguro, M. Rathaiah, K. Linganna, A.D. Lozano-Gorrín, M.A. Hernández-Rodríguez, I.R. Martín, P. Babu, U.R. Rodríguez-Mendoza, F.J. Manjón, A. Muñoz, C.K. Jayasankar, V. Venkatramu, V. Lavín, Chemical pressure effects on the spectroscopic properties of Nd^{3+}-doped gallium nanogarnets, Opt. Mater. Express 5 (2015) 1661–1673, https://doi.org/10.1364/OME.5.001661.
[12] S.F. León-Luis, U.R. Rodríguez-Mendoza, I.R. Martín, E. Lalla, V. Lavín, Effects of Er^{3+} concentration on thermal sensitivity in optical temperature fluorotellurite glass sensors, Sensor. Actuator. B Chem. 176 (2013) 1167–1175, https://doi.org/10.1016/j.snb.2012.09.067.
[13] L. Aigouy, E. Saïdi, L. Lalouat, J. Labéguerie-Egéa, M. Mortier, P. Löw, C. Bergaud, AC thermal imaging of a microwire with a fluorescent nanocrystal: influence of the near field on the thermal contrast, J. Appl. Phys. 106 (2009), https://doi.org/10.1063/1.3233940, 074301.

[14] B. Samson, L. Aigouy, G. Tessier, P. Löw, B.J. Kim, C. Bergaud, M. Mortier, Thermal imaging of nickel wires with a fluorescent nanoprobe, J. Phys. Conf. Ser. 92 (2007) 1–4, https://doi.org/10.1088/1742-6596/92/1/012089.
[15] Z.P. Cai, H.Y. Xu, Point temperature sensor based on green upconversion emission in an Er:ZBLALiP microsphere, Sensors Actuators A Phys 108 (2003) 187–192, https://doi.org/10.1016/j.sna.2003.07.008.
[16] C. Li, B. Dong, C. Ming, M. Lei, Application to temperature sensor based on green up-conversion of Er^{3+} doped silicate glass, Sensors 7 (2007) 2652–2659, https://doi.org/10.3390/s7112652.
[17] P. Haro-González, S.F. León-Luis, S. González-Pérez, I.R. Martín, Analysis of Er^{3+} and Ho^{3+} codoped fluoroindate glasses as wide range temperature sensor, Mater. Res. Bull. 46 (2011) 1051–1054, https://doi.org/10.1016/j.materresbull.2011.03.010.
[18] J. Cao, W. Chen, D. Xu, F. Hu, L. Chen, H. Guo, Wide-range thermometry based on green up-conversion of Yb^{3+}/Er^{3+} co-doped KLu_2F7 transparent bulk oxyfluoride glass ceramics, J. Lumin. 194 (2018) 219–224, https://doi.org/10.1016/j.jlumin.2017.10.020.
[19] M. Runowski, N. Stopikowska, D. Szeremeta, S. Goderski, M. Skwierczyńska, S. Lis, Upconverting lanthanide fluoride Core@Shell nanorods for luminescent thermometry in the first and second biological windows: β-NaYF 4 : Yb^{3+}–Er^{3+} @SiO_2 temperature sensor, ACS Appl. Mater. Interfaces 11 (2019) 13389–13396, https://doi.org/10.1021/acsami.9b00445.
[20] H. Berthou, C.K. Jörgensen, Optical-fiber temperature sensor based on upconversion-excited fluorescence, Opt. Lett. 15 (1990) 1100–1102, https://doi.org/10.1364/OL.15.001100.
[21] W. Xu, H. Zhao, Y. Li, L. Zheng, Z. Zhang, W. Cao, Optical temperature sensing through the upconversion luminescence from Ho^{3+}/Yb^{3+} codoped CaWO4, Sensor. Actuator. B Chem. 188 (2013) 1096–1100, https://doi.org/10.1016/j.snb.2013.07.094.
[22] R. Dey, A. Kumari, A.K. Soni, V.K. Rai, CaMoO4:Ho^{3+}–Yb^{3+}–Mg^{2+} upconverting phosphor for application in lighting devices and optical temperature sensing, Sensor. Actuator. B Chem. 210 (2015) 581–588, https://doi.org/10.1016/j.snb.2015.01.007.
[23] P. Singh, P.K. Shahi, A. Rai, A. Bahadur, S.B. Rai, Effect of Li^{+} ion sensitization and optical temperature sensing in Gd 2 O 3 : Ho^{3+}/Yb^{3+}, Opt. Mater. 58 (2016) 432–438, https://doi.org/10.1016/j.optmat.2016.06.010.
[24] M. Kamimura, T. Matsumoto, S. Suyari, M. Umezawa, K. Soga, Ratiometric near-infrared fluorescence nanothermometry in the OTN-NIR (NIR II/III) biological window based on rare-earth doped β-$NaYF_4$ nanoparticles, J. Mater. Chem. B. 5 (2017) 1917–1925, https://doi.org/10.1039/C7TB00070G.
[25] L. Wortmann, S. Suyari, T. Ube, M. Kamimura, K. Soga, Tuning the thermal sensitivity of β-NaYF4: Yb^{3+}, Ho^{3+}, Er^{3+} nanothermometers for optimal temperature sensing in OTN-NIR (NIR II/III) biological window, J. Lumin. 198 (2018) 236–242, https://doi.org/10.1016/j.jlumin.2018.01.049.
[26] X. Wang, Q. Liu, Y. Bu, C.-S. Liu, T. Liu, X. Yan, Optical temperature sensing of rare-earth ion doped phosphors, RSC Adv. 5 (2015) 86219–86236, https://doi.org/10.1039/C5RA16986K.
[27] P. Haro-González, S.F. León-Luis, S. González-Pérez, I.R. Martín, Analysis of Er^{3+} and Ho^{3+} codoped fluoroindate glasses as wide range temperature sensor, Mater. Res. Bull. 46 (2011) 1051–1054, https://doi.org/10.1016/j.materresbull.2011.03.010.
[28] I.R. Martín, V.D. Rodríguez, R. Alcalá, R. Cases, Cross-relaxation for Tm^{3+} ions in indium-based glasses, J. Non-Cryst. Solids 161 (1993) 294–296, https://doi.org/10.1016/0022-3093(93)90721-9.
[29] S.A. Wade, S.F. Collins, G.W. Baxter, Fluorescence intensity ratio technique for optical fiber point temperature sensing, J. Appl. Phys. 94 (2003) 4743–5756, https://doi.org/10.1063/1.1606526.
[30] I.R. Martin, V.D. Rodriguez, M. Morales, U.R. Rodriguez-Mendoza, V. Lavin, Excited-state dynamics in Yb^{3+}-Ho^{3+}-doped fluoroindate glasses, J. Appl. Spectrosc. 62 (1995) 865–871, https://doi.org/10.1007/BF02606652.
[31] C.D.S. Brites, A. Millán, L.D. Carlos, Lanthanides in luminescent thermometry, Handb. Phys. Chem. Rare Earths 49 (2016) 339–427, https://doi.org/10.1016/bs.hpcre.2016.03.005.
[32] C.A. Morrison, R.P. Leavitt, Spectroscopic properties of triply ionized, in: Handb. Phys. Chem. Rare Earths, 1982, pp. 461–692, https://doi.org/10.1016/S0168-1273(82)05009-0.
[33] C.D.S. Brites, K. Fiaczyk, J.F.C.B. Ramalho, M. Sójka, L.D. Carlos, E. Zych, Widening the temperature range of luminescent thermometers through the intra- and interconfigurational transitions of Pr^{3+}, Adv. Opt. Mater. 6 (2018) 1–5, https://doi.org/10.1002/adom.201701318.
[34] G. Jiang, X. Wei, S. Zhou, Y. Chen, C. Duan, M. Yin, Neodymium doped lanthanum oxysulfide as optical temperature sensors, J. Lumin. 152 (2014) 156–159, https://doi.org/10.1016/j.jlumin.2013.10.027.
[35] M.G. Nikolić, A.Z. Al-Juboori, V. Đorđević, M.D. Dramićanin, Temperature luminescence properties of Eu^{3+}–doped Gd_2O_3 phosphors, Phys. Scripta T157 (2013) 1–5, https://doi.org/10.1088/0031-8949/2013/T157/014056.
[36] M.G. Nikolić, D.J. Jovanović, M.D. Dramićanin, Temperature dependence of emission and lifetime in Eu^{3+}–and $Dy^{3}+$ -doped $GdVO_4$, Appl. Optic. 52 (2013) 1716–1724, https://doi.org/10.1364/AO.52.001716.
[37] R. Shi, L. Lin, P. Dorenbos, H. Liang, Development of a potential optical thermometric material through photoluminescence of Pr^{3+} in La_2 $MgTiO_6$, J. Mater. Chem. C. 5 (2017) 10737–10745, https://doi.org/10.1039/C7TC02661G.
[38] Y.L. Hu, Z.Y. Zhang, K.T.V. Grattan, A.W. Palmer, B.T. Meggitt, Ruby-based decay-time thermometry: effect of probe size on extended measurement range (77–800 K), Sensors Actuators A Phys 63 (1997) 85–90, https://doi.org/10.1016/S0924-4247(97)01523-9.
[39] Z. Zheng, J. Zhang, X. Liu, R. Wei, F. Hu, H. Guo, Luminescence and self-referenced optical temperature sensing performance in $Ca_2YZr_2Al_3O_{12}$: Bi^{3+},Eu^{3+} phosphors, Ceram. Int. 46 (2020) 6154–6159, https://doi.org/10.1016/j.ceramint.2019.11.081.
[40] H. Peng, H. Song, B. Chen, J. Wang, S. Lu, X. Kong, J. Zhang, Temperature dependence of luminescent spectra and dynamics in nanocrystalline Y_2O_3: Eu^{3+}, J. Chem. Phys. 118 (2003) 3277–3282, https://doi.org/10.1063/1.1538181.
[41] W. Stręk, C. Szafrański, E. Łukowiak, Z. Mazurak, B. Jeżowska-Trzebiatowska, Fluorescence quenching in neodymium pentaphosphate, Phys. Status Solidi 41 (1977) 547–553, https://doi.org/10.1002/pssa.2210410226.
[42] M.J. Weber, Luminescence decay by energy migration and transfer: observation of diffusion-limited relaxation, Phys. Rev. B 4 (1971) 2932–2939, https://doi.org/10.1103/PhysRevB.4.2932.
[43] H.J. Lozykowski, W.M. Jadwisienczak, Thermal quenching of luminescence and isovalent trap model for rare-earth-ion-doped AlN, Phys. Status Solidi 244 (2007) 2109–2126, https://doi.org/10.1002/pssb.200642152.